Journal of Advanced Ceramics
2020, **9**(2): 193–203
https://doi.org/10.1007/s40145-020-0359-8

ISSN 2226-4108
CN 10-1154/TQ

Research Article

Fabrication, microstructure, and properties of SiC/Al_4SiC_4 multiphase ceramics via an *in-situ* formed liquid phase sintering

Junwen LIU[a,b], Xiaobing ZHOU[b,*], Peter TATARKO[c], Qin YUAN[b], Lan ZHANG[a], Hongjie WANG[a], Zhengren HUANG[b], Qing HUANG[b]

[a]*State Key Laboratory for Mechanical Behavior of Materials*, *Xi'an Jiaotong University*, *Xi'an 710049*, *China*
[b]*Engineering Laboratory of Advanced Energy Materials*, *Ningbo Institute of Materials Technology and Engineering*, *Chinese Academy of Sciences*, *Ningbo 315201*, *China*
[c]*Institute of Inorganic Chemistry*, *Slovakia Academy of Sciences*, *Dúbravská cesta 9,845 36 Bratislava 45*, *Slovakia*

Received: September 16, 2019; Revised: December 29, 2019; Accepted: January 6, 2020

Abstract: The SiC/Al_4SiC_4 composites with the improved mechanical properties and thermal conductivity were fabricated by the *in-situ* reaction of polycarbosilane (PCS) and Al powders using spark plasma sintering. The addition of 5 wt% yttrium (Y) sintering additive was useful to obtain fully dense samples after sintering at a relatively low temperature of 1650 ℃, due to the formation of a liquid phase during sintering. The average particle size of the *in-situ* formed SiC was ~300 nm. The fracture toughness (4.9 MPa·$m^{1/2}$), Vickers hardness (16.3 GPa), and thermal conductivity (15.8 W/(m·K)) of the SiC/Al_4SiC_4 composite sintered at 1650 ℃ were significantly higher than the hardness (13.2 GPa), fracture toughness (2.16 MPa·$m^{1/2}$), and thermal conductivity (7.8 W/(m·K)) of the monolithic Al_4SiC_4 ceramics. The improved mechanical and thermal properties of the composites were attributed to the high density, fine grain size, as well as the optimized grain boundary structure of the SiC/Al_4SiC_4 composites.

Keywords: Al_4SiC_4; SiC; $Y_3Si_2C_2$; spark plasma sintering

1 Introduction

Aluminum silicon carbide (Al_4SiC_4) is ternary layered ceramics with hexagonal structure symmetry of space group $P6_3mc$ (No. 186), in which the Al_4C_3-type and SiC-type sub-units are alternatively stacked along the *c*-axis direction [1]. Al_4SiC_4 has good combination of properties, such as low density (3.03 g/cm^3), high melting point (2080 ℃), high compressive strength (260 GPa), as well as remarkable resistance to oxidation, corrosion, and hydration at high temperatures [2–6]. Due to its good oxidation resistance in the saturated water vapor environments [7,8], high strength at elevated temperatures [9], and excellent slag corrosion resistance [10,11], Al_4SiC_4 has potential to be used in aerospace and nuclear applications. However, its relatively low hardness (10.6 GPa) and fracture toughness (3.98 MPa·$m^{1/2}$) [9] may limit its application [6].

One efficient way to improve hardness, fracture toughness, and thermal conductivity of Al_4SiC_4 is to incorporate a reinforcing filler with high thermal

* Corresponding author.
E-mail: zhouxb@nimte.ac.cn

conductivity into the Al_4SiC_4 matrix. Silicon carbide (SiC) is a promising candidate, because of its high hardness, excellent mechanical properties at high temperatures, and high thermal conductivity [12–15]. The SiC particles have successfully been used to reinforce titanium silicon carbide (Ti_3SiC_2) matrices [16–18]. Zhang *et al*. [18] reported that the hardness, fracture toughness, and thermal conductivity of Ti_3SiC_2 were improved by the addition of SiC nano particles into the Ti_3SiC_2 matrix. Therefore, the motivation of the present work was to utilize the reinforcing effect of SiC nano particles to develop the SiC/Al_4SiC_4 composites with improved mechanical properties and thermal conductivity.

Pure Al_4SiC_4 can be synthesized using different methods and starting materials, which mainly include: 1) solid-state reactions of the starting mixture containing aluminum, silicon, and carbon powders [6,19,20]; 2) solid-state reactions of the aluminum, carbon, and polycarbosilane (PCS) starting mixture, in which PCS replaces Si as the source of Si and C [9]; 3) solid-state reactions of the starting Al_4C_3 and SiC powders [21,22]; 4) carbothermal reduction of the Al_2O_3 or $Al(OH)_3$, SiO_2, and C powder mixture [23,24].

Among all of these methods, the one that uses PCS as a raw material attracted our attention to develop SiC/Al_4SiC_4 composites. This is because the nano sized SiC particles, which are beneficial for toughening the Al_4SiC_4 materials, could be derived from PCS. On the other hand, the densification of Al_4SiC_4 is usually performed at high temperatures, around 1900 ℃ [9]. The use of sintering additives is necessary to reduce the sintering temperature. Recently, yttrium silicon carbide ($Y_3Si_2C_2$) was successfully used as the sintering additive for SiC [25] and predicted as a promising interphase material with great interest for SiC_f/SiC composites [26]. According to the calculated Y–Si–C ternary phase diagram, a liquid phase is formed at the temperatures of ~1560 ℃ [25]. The presence of the liquid phase effectively promotes densification of SiC ceramics. Furthermore, an eutectic liquid phase can also be formed in the Y_2O_3–Al_2O_3–SiO_2 system at the temperature of ~1640 ℃ [27]. From this point of view, two different liquid phases may form during sintering of SiC/Al_4SiC_4 with the yttrium (Y) additive. This would significantly promote the densification of SiC/Al_4SiC_4.

Therefore, PCS and Al powders were used in the present study to form Al_4SiC_4 ceramics with the *in-situ* formed SiC particles. 5 wt% Y was used as the sintering additive to enable densification of the SiC/Al_4SiC_4 composites at relatively low temperatures. The aim of this study was to investigate the densification mechanism of SiC/Al_4SiC_4 composites, and to understand the effect of the nano-sized SiC on the mechanical properties and thermal conductivity of SiC/Al_4SiC_4 composites. This is the first study to develop highly dense SiC/Al_4SiC_4 composites using a rare earth element as the sintering additive. The newly developed SiC/Al_4SiC_4 composites may combine the individual advantages of SiC and Al_4SiC_4 ceramics, making the SiC/Al_4SiC_4 materials of great interest for aerospace and nuclear applications.

2 Experimental

2. 1 Materials

The PCS powder with an average molecular weight of ~1500 was used as the raw material. It was synthesized by heating polydimethylsilane (PDMS) at the temperature of 455 ℃ under an external pressure of 16 MPa, according to the approach proposed by Hasegawa *et al*. [28,29]. The Al powder (99% purity, Sinopharm Chemical Reagent Co., Ltd., Shanghai, China) with a particle size of 75–150 μm was also used as the raw material. In addition, the Y powder (Sinopharm Chemical Reagent Co., Ltd., Shanghai, China) with a purity of 99.5% and a mean particle size of 75 μm was used as the sintering additive. The commercially available graphite powder (300 mesh, 99.5% purity) was obtained from Aladdin Chemical Reagent, China. The β-SiC powder (99.5%, Eno Material Co., Ltd., Qinhuangdao, China) with a mean particle size of 0.5 μm was used to synthesize the reference, pure Al_4SiC_4 sample.

2. 2 Composite preparation

As-synthesized PCS powder was cross-linked at 600 ℃ for 2 h in a flowing Ar atmosphere. The weight fractions of Si, C, and O in the as-obtained cross-linked PCS were 55.45%, 40.1%, and 4.5%, respectively. The amount of free carbon was calculated to be ~18 wt%, assuming that all oxygen was in the form of SiO_2 in the cross-linked PCS powder. The cross-linked PCS powder was subsequently mixed with the Al powder. In order to form Al_4C_3, the molar ratio of Al:C in the cross-linked PCS powder was 4:3. The powder mixture

was then pyrolysized at 1000 ℃ for 30 min in an Ar atmosphere. The sample was referred as S1000. The weight fraction of SiC in the final SiC/Al_4SiC_4 materials was calculated to be 45.4 wt% (43.9 vol%), assuming that all Al transformed to Al_4SiC_4.

The amount of 5 wt% Y was added to the S1000 sample as the sintering additive. Sintering of the powder mixture was performed in a spark plasma sintering (SPS) furnace (HPD 25/1, FCT systems, Germany) using an Ar atmosphere. The heating rate was 50 ℃/min up to the temperature of 1400 ℃, while it was decreased to 25 ℃/min for the temperatures above 1400 ℃. The applied uniaxial pressure was increased from 16 to 64 MPa within the first 5 min at the target temperature, followed by the dwell time of additional 5 min at the target temperature. The materials were sintered at different target temperatures, i.e., 1200 ℃ (S1200), 1400 ℃ (S1400), 1500 ℃ (S1500), 1550 ℃ (S1550), 1600 ℃ (S1600), and 1650 ℃ (S1650). For the sake of comparison, the SiC/Al_4SiC_4 sample without Y additive was sintered using the same conditions as used for the S1650 sample, and was referred as S1650-C. At the same time, the reference monolithic Al_4SiC_4 sample was also prepared by the SPS sintering of Al_4C_3 and SiC powders at the temperature of 1900 ℃ for 20 min with a uniaxial pressure of 32 MPa. The Al_4C_3 powder was synthesized using pure Al and C powders (with the molar ratio of Al:C = 4:3) at 1200 ℃ for 2 h in an Ar atmosphere.

2. 3 Material characterization

The phase composition of the composites was determined by an X-ray diffractometer (XRD, D8 Advance; Bruker AXS, Karlsrude, Germany) using a Cu Kα radiation (λ = 1.5406 Å). The microstructure and the fracture surfaces of the specimens were performed using a scanning electron microscope (SEM, FEI Quanta FEG 250), equipped with an energy dispersive spectroscopy (EDS) detector.

The apparent densities of the composites were measured using an Archimedes' method. The porosity of the samples was determined using a High-Performance Full-Automatic Mercury Intrusion Meter (AutoPore IV 9510, micrometrics instrument corporation, USA). The hardness measurements were carried out using a Vickers' diamond indenter (HVs-1000 Digital micro Vickers' Hardness Tester, Beijing Times Mountain Peak Technology Co., Ltd., Beijing, China). An indentation load (P) of 9.8 N and a dwell time of 15 s were used. At least 20 indents were measured for each specimen. The elastic modulus was measured using a nanoindentation system (Hysitron PI85, Bruker) on the polished samples. The indentation fracture toughness (K_{IC}) was determined by the measuring of the length of the cracks introduced by Vickers indentation at the load of 9.8 N. The fracture toughness was then calculated using Eq. (1), according to Refs. [30,31]:

$$K_{IC} = 0.016(E/H)^{1/2}PC^{-3/2} \quad (1)$$

where E is the elastic modulus, H is the indentation hardness, and C is the half-length of the cracks, measured using SEM.

The laser flash method was used to measure the thermal diffusivity and specific heat capacity using a Netzsch LFA 457 apparatus (LFA, NETZSCH-Gerätebau GmbH, Germany). The thermal conductivity (κ, W/(m·K)) was calculated according to Eq. (2) [32]:

$$\kappa = \alpha\rho C_p \quad (2)$$

where α is the coefficient of thermal diffusivity, ρ is the density of the material, and C_p is the specific heat capacity.

3 Results and discussion

3. 1 Microstructure of SiC/Al_4SiC_4 composites and Al_4SiC_4

The relative densities of the SiC/Al_4SiC_4 composites sintered at different temperatures are shown in Table 1. The relative density significantly increased from 67.4% to 98.6% when the sintering temperature was increased from 1400 to 1650 ℃ for the sample with 5 wt% Y additive. On the other hand, the relative density was only 89.9% for the sample sintered at 1650 ℃ without Y additive (S1650-C). This clearly indicates that the Y additive promoted densification of the SiC/Al_4SiC_4 composites, probably due to formation of a liquid phase.

Figure 1 shows the XRD patterns of the pyrolyzed powder (S1000) and all the samples sintered at different temperatures. The following phases: Al_4C_3 (JCPDS card No. 35-0799), Al–Si alloy (JCPDS card No. 41-1222), and β-SiC (JCPDS card No. 29-1129) were detected for the pyrolyzed powder (S1000). The broad diffraction peak of the β-SiC phase suggests an incomplete crystallization of SiC at 1000 ℃, according

Table 1 Chemical composition, density, grain size of SiC particles, mechanical and thermal properties of the investigated SiC/Al_4SiC_4 multiphase ceramics and Al_4SiC_4 monoliths

Sintering temp. (℃)	Phases	Density ($g·cm^{-3}$)	Relative density	Grain size of SiC (nm)	Vickers hardness (GPa)	Elastic modulus (GPa)	Fracture toughness ($MPa·m^{1/2}$)	Thermal conductivity (W/(m·K))
1500	$Y_3Al_5O_{12}$; SiC; Al_4SiC_4; $Y_2Si_2O_7$	2.894	92.9	66±8.6	—	—	—	5.6±0.01
1550	$Y_3Al_5O_{12}$; SiC; Al_4SiC_4	2.923	93.8	103±16	—	—	—	11.1±0.03
1600	$Y_3Al_5O_{12}$; SiC; Al_4SiC_4	2.933	93.9	153±25	15.3±1.9	235.4±0.5	3.6±0.4	14.1±0.05
1650	$Y_3Al_5O_{12}$; SiC; Al_4SiC_4	3.069	98.6	304±33	16.3±0.6	218.4±1.1	4.9±0.2	15.8±0.02
1650-C	SiC; Al_4SiC_4; Al_4O_4C	2.955	89.9	131±16	19.1±1.5	233.8±2.0	2.7±0.09	9.6±0.03
1900	Al_4SiC_4	2.997	98.9	7.3±0.7 μm	13.2±0.9	192.1±1.68	2.16±0.15	7.8±0.02
1900 [9]	Al_4SiC_4	2.97 [9]	98.0 [9]	2–5 μm [9]	10.6±1.8 [9]	—	3.98±0.05 [9]	—

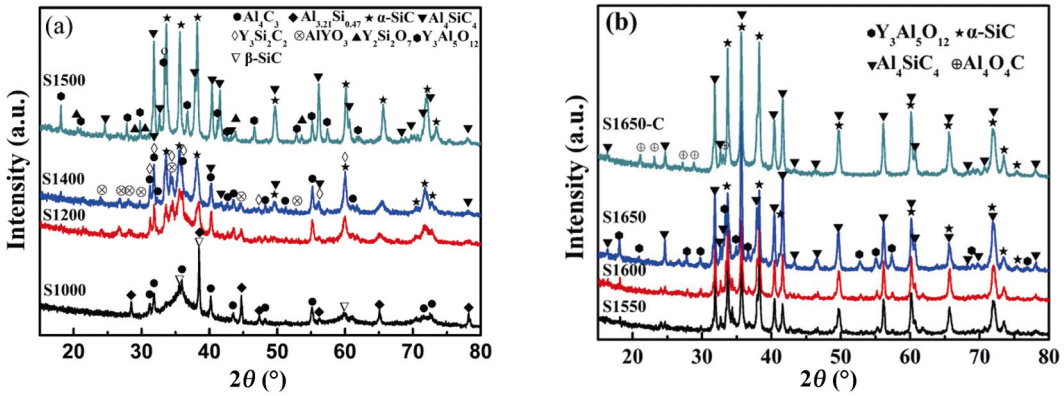

Fig. 1 XRD patterns of the pyrolyzed powder (S1000) and the samples sintered at different temperatures.

to Reaction (3) [9]. The presence of the Al_4C_3 phase can be explained by the reaction of molten Al (~660 ℃) with free carbon, according to Reaction (4) [9]. On the other hand, some remaining Al could also react with SiC to form Al_4C_3 and Si, according to Reaction (5) [33]. The Al–Si alloy could be subsequently formed by the dissolution of Si into the unreacted Al, according to Reaction (6) [33]. The main possible reactions could be summarized as follows:

$$\text{PCS} \rightarrow \text{SiC} + \text{C} + \text{gas}\uparrow \quad (3)$$

$$4\text{Al} + 3\text{C} \rightarrow \text{Al}_4\text{C}_3 \quad (4)$$

$$4\text{Al} + 3\text{SiC} \rightarrow \text{Al}_4\text{C}_3 + 3\text{Si} \quad (5)$$

$$x\text{Al} + y\text{Si} \rightarrow \text{Al}_x\text{Si}_y \quad (6)$$

When the calcined powder with the Y additive was sintered at 1200 ℃, Al_4SiC_4 (JCPDS card No. 35-1072), $Y_3Si_2C_2$ (JCPDS card No. 51-0835), and $YAlO_3$ impurity (JCPDS card No. 33-0041) were detected by XRD. Some residual unreacted SiC (JCPDS card No. 29-1126) and Al_4C_3 were also found (Fig. 1(a)). It should be mentioned that the β- to α- phase transformation of SiC was observed. This might have been caused by the dissolution of Al into the SiC grains, which promotes the β-to-α phase transformation of SiC [34,35]. The Al_4SiC_4 phase could be formed at the temperatures above 1106 ℃, according to the pseudo binary phase diagram of the Al_4C_3–SiC system [19]. The formation of $Y_3Si_2C_2$ occurred by the reaction between Y and SiC, according to Reaction (8) [36]. There were no new, additional phases detected when the sintering temperature was increased to 1400 ℃. The main possible reactions in the temperature range of 1200–1400 ℃ could be summarized as follows:

$$\text{Al}_4\text{C}_3 + \text{SiC} \rightarrow \text{Al}_4\text{SiC}_4 \quad (7)$$

$$3\text{Y} + 2\text{SiC} \rightarrow \text{Y}_3\text{Si}_2\text{C}_2 \quad (8)$$

When the sintering temperature increased to 1500–1600 ℃, the diffraction peaks of $Y_3Si_2C_2$ were no longer observed in the XRD patterns. This was caused by the formation of a liquid phase, which forms at the temperatures around 1560 ℃ via a ternary eutectic Reaction (9), according to the calculated Y–Si–C ternary phase diagram [36]. In Reaction (9), "L" represents the liquid phase and "γ" represents the binary Y–C compound [36]. In addition, the decomposition of $Y_3Si_2C_2$ led to the formation of Y-based liquid, according to Reaction (10) [36]. The Y-based liquid

could later oxidize by its reaction with oxygen from the composites, according to Reaction (11) [25]. Thus, the main possible reactions could be described as follows:

$$L \rightleftharpoons SiC + \gamma + Y_3Si_2C_2 \quad (9)$$

$$Y_3Si_2C_2 \rightarrow 2SiC + 3Y(l) \quad (10)$$

$$4Y(l) + O_2 \rightarrow 2Y_2O_3 \quad (11)$$

When the temperature further increased to 1650 ℃, the relative intensities of the SiC diffraction peaks increased significantly. This was caused by the growth of the SiC grains. According to the calculated phase diagram, an eutectic liquid phase is formed in the Y_2O_3–Al_2O_3–SiO_2 system at the temperatures between 1635 and 1644 ℃ by Reactions (12) and (13) [27]. Furthermore, Liang *et al*. [37] reported that a liquid phase was clearly observed in the pressureless sintered SiC with Al_2O_3 and Y_2O_3 additives at the temperature of 1680 ℃. The presence of a liquid phase improves the atoms diffusion and promotes the grain growth of SiC. On the other hand, a certain amount of an amorphous silicate phase (could not be detected by XRD) might have been formed by the reactions between the additives and the silica layer present on the surface of SiC, as observed by Falk [38].

$$L + Y_4Al_2O_9 \rightleftharpoons Y_2SiO_5 + Y_3Al_5O_{12} \quad (12)$$

$$L + YAlO_3 + Y_4Al_2O_9 \rightleftharpoons Y_3Al_5O_{12} \quad (13)$$

Moreover, the relative X-ray intensities of the (001) planes of Al_4SiC_4 increased with the increasing sintering temperature. The relative ratio of the (00 10) and (1$\bar{1}$0) planes (I(00 10)/I(1$\bar{1}$0)) of Al_4SiC_4 increased from 0.9 to 1.5 when the sintering temperature increased from 1500 to 1650 ℃. This relative ratio is much higher than the ratio calculated from the standard JCPDS card (I(00 10)/I(1$\bar{1}$0) = 0.76). This indicates that preferential grain growth orientation was obtained. Xing *et al*. [4] observed similar phenomena during the synthesis of Al_4SiC_4 powder by the carbothermal reduction method.

The sample sintered without Y additive (S1650-C) contained the following crystalline phases: SiC, Al_4SiC_4, and the impurity of Al_4O_4C. The formation of Al_4O_4C can be possible explained by the reduction of Al_2O_3 by its reaction with C (Reaction (14)), as well as to the reaction between Al_2O_3 and Al_4C_3 (Reaction (15)) [9, 19].

$$2Al_2O_3 + 3C \rightarrow Al_4O_4C + 2CO(g) \quad (14)$$

$$4Al_2O_3 + Al_4C_3 \rightarrow 3Al_4O_4C \quad (15)$$

For the sake of comparison, the monolithic Al_4SiC_4 was also prepared. Figure 2(a) shows the XRD patterns of both the Al_4C_3 powder as the raw material, and the as-obtained pure Al_4SiC_4 ceramics. No impurity was detected. The SEM analysis of the fracture surface revealed the presence only a few micro-pores (Fig. 2(b)), suggesting that a high dense Al_4SiC_4 material (98.9%) was obtained.

To further understand the effect of Y additive on the sintering of SiC/Al_4SiC_4 composites and reveal the densification mechanism, the fracture surfaces of the samples sintered at different temperatures (Figs. 3 and 4) were observed. Obviously, the microstructure of the S1400 sample was significantly porous, and the agglomeration of SiC particles was also observed (Figs. 3(a) and 4(a)). The number of pores significantly decreased when the sintering temperature increased to 1500 ℃ (Fig. 3(b)). No obvious change in number of pores was observed when the sintering temperature was increased to 1550 and 1600 ℃ (Figs. 3(c) and 3(d)). However, some abnormal growth of Al_4SiC_4 grains was observed at these temperatures (Figs. 4(c) and 4(d)). The pores were always located around the large Al_4SiC_4 grains.

A significantly different morphology of the fracture surface was observed for the specimen S1650 (Fig. 3(e)).

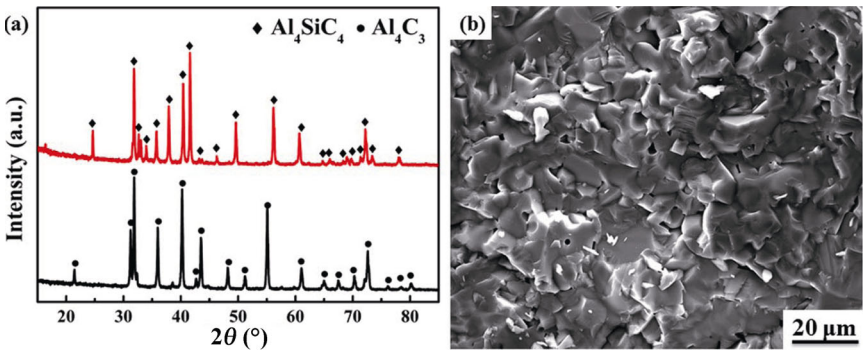

Fig. 2 (a) XRD patterns of the Al_4C_3 powder and pure Al_4SiC_4 sintered at 1900 ℃; (b) SEM image of the fracture surface of pure Al_4SiC_4 ceramics.

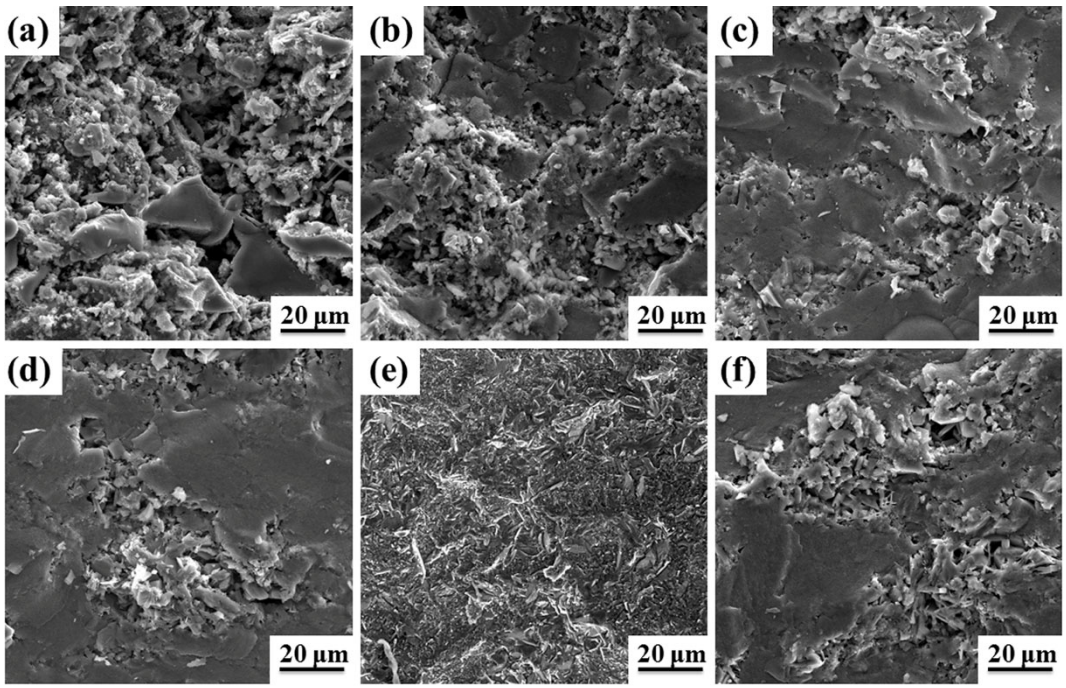

Fig. 3 Low magnification SEM images of the fracture surfaces of the SiC/Al_4SiC_4 sintered at different temperatures: (a) S1400, (b) S1500, (c) S1550, (d) S1600, (e) S1650, and (f) S1650-C (without Y additive).

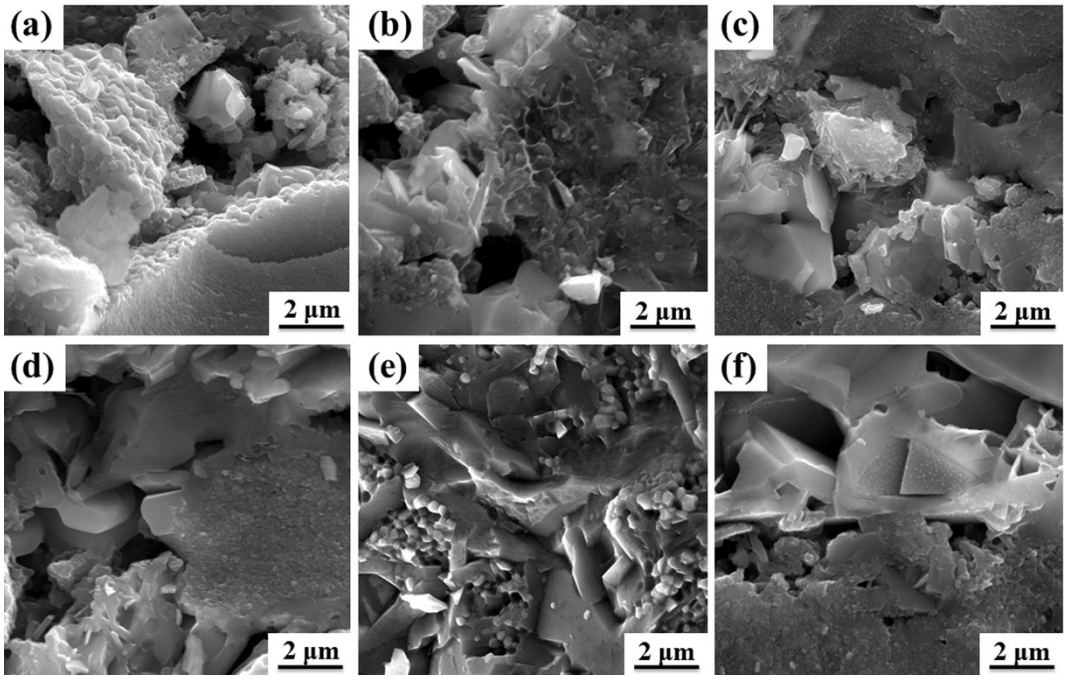

Fig. 4 High magnification SEM images of the fracture surfaces of the SiC/Al_4SiC_4 sintered at different temperatures: (a) S1400, (b) S1500, (c) S1550, (d) S1600, (e) S1650, and (f) S1650-C (without Y additive).

The SEM analysis revealed the presence of a rough surface, resulting from the grains pull out. No obvious porosity was observed. On the other hand, the fracture surface of the S1650-C sample sintered without Y additive was relatively smooth (Figs. 3(f) and 4(f)). Numerous pores and abnormal growth of Al_4SiC_4 grains were observed. Such a significantly different fracture surface morphology was caused by a large amount of the liquid phase formed in the temperature range of 1600–1650 ℃ when Y sintering additive was

used (the sample S1650) [27,37]. The large amount of the liquid phase not only filled up the pores between the large plate-like Al_4SiC_4 grains (Figs. 3(e) and 4(e)), but also improved the diffusion of atoms along the grain boundaries [39,40]. Therefore, the relative density of the S1650 (98.6%) was significantly higher than that of the S1650-C (89.9%).

Figure 5 shows the typical low and high magnification back-scattered electron (BSE) SEM images of the samples S1500, S1600, and S1650. In the case of the samples sintered at 1500 and 1600 ℃, the Y-rich amorphous glassy phase (bright phase) formed by solidification of a liquid upon cooling from the sintering temperature, was localized in the porous area between the large Al_4SiC_4 grains (Figs. 5(a), 5(b), 5(d), and 5(e)). However, the liquid phase was homogenously dispersed when the sintering temperature was increased to 1650 ℃. Most of the Y-rich amorphous phase was located at the grain boundaries (Figs. 5(c) and 5(f)). The uniform dispersion of the glassy phase at the grain boundaries would play an important role for the mechanical properties of the composites.

3. 2 *In-situ* reaction and densification process

According to the phase and microstructure evolution, the *in-situ* reaction and sintering process of SiC/Al_4SiC_4 composites can be divided into four stages, as schematically shown in Fig. 6. In the initial stage (≤ 1400 ℃), the Al_4SiC_4 and $Y_3Si_2C_2$ phases were formed via Reactions (7) and (8). There was no liquid phase formed, so any densification occurred via solid-state mechanism. The formation of the large, interconnected pores in the sintered body was characteristic for this stage. As the sintering temperature increased to 1500 ℃, $Y_3Si_2C_2$ transformed to a liquid phase by Reaction (9). The liquid phase wetted and covered the SiC particles. The grains of SiC and Al_4SiC_4 dissolved in the liquid phase, resulting in the particles rearrangement. In the temperature range of 1500–1600 ℃, the sintering occurred via solution and re-precipitation process. However, the densification was limited by the formation of a small amount of the liquid phase at this temperature range.

When the sintering temperature increased to 1650 ℃, a large amount of the liquid phase was formed by Reactions (12) and (13). The sufficient amount of the liquid phase not only filled the pores, but also promoted the diffusion of atoms along the grain boundaries [39]. Furthermore, the coarsening of the SiC and Al_4SiC_4 grains occurred via the solution-re-precipitation mechanism. At high temperatures, the solubility of C, Si, and Al in the liquid phase increases, due to the large capillary forces. Thus, the fine SiC and Al_4SiC_4 grains dissolved into the liquid, and re-precipitated onto the surface of larger SiC and Al_4SiC_4

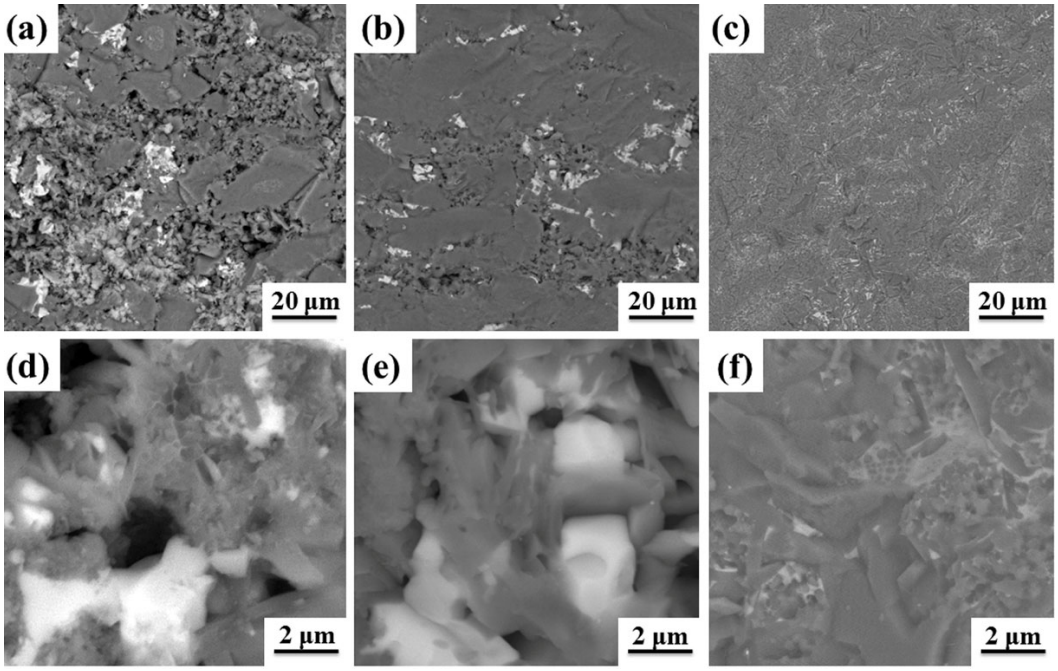

Fig. 5 Typical low and high magnification BSE SEM images of the fracture surfaces of SiC/Al_4SiC_4 showing the distribution of the Y-rich phase sintered at: (a, d) 1500 ℃; (b, e) 1600 ℃; (c, f) 1650 ℃.

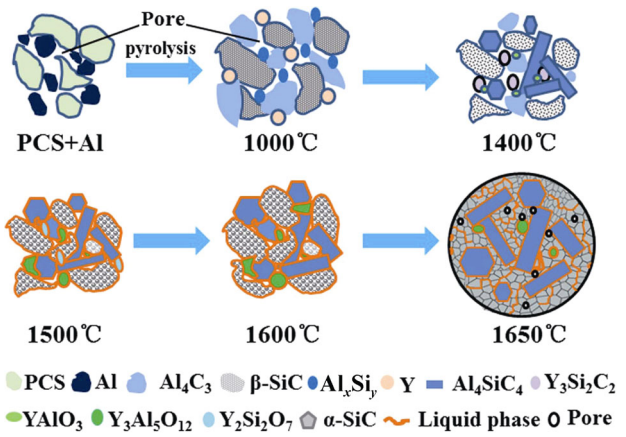

Fig. 6 Schematic diagram of the *in-situ* reaction and densification process of SiC/Al_4SiC_4 composites at different sintering temperatures.

grains. The initial grains of SiC and Al_4SiC_4 acted as nuclei for the growth of large grains via Oswald ripening mechanism [40]. Therefore, the mean grain size of the SiC particles significantly increased from 153 to 304 nm when the temperature increased from 1600 to 1650 ℃.

3. 3 Mechanical properties

Table 1 shows the Vickers hardness, elastic modulus, and K_{IC} of the SiC/ Al_4SiC_4 composites sintered at different temperatures. For the sake of comparison, the mechanical properties of the monolithic Al_4SiC_4 material are also given in Table 1. The Vickers hardness increased from 15.3 ± 1.9 (S1600) to 16.3 ± 0.6 GPa (S1650), as the density increased with the increasing sintering temperature. However, the hardness of the sample without Y additive (S1650-C) was higher than that of the S1650 sample, even though the S1650-C sample exhibited a lower relative density than the S1650 sample. This can be attributed to the finer grain size of the SiC particles in the S1650-C (131 nm) sample, when compared to the S1650 sample (304 nm). Another reason of the lower hardness of the S1650 sample was that it contained a relatively large amount of the grain boundary glassy phase, which has a significantly lower hardness than the crystalline ceramic grains [40]. The hardness of the SiC/Al_4SiC_4 composite sintered at 1650 ℃ (16.3 GPa) was significantly higher when compared to the pure Al_4SiC_4 material (13.2 GPa). This can be explained by the presence of SiC particles with a relatively high intrinsic hardness (25 GPa [40]). Since the open porosity of the S1650 sample (6.5%) was at the similar level than that of the pure Al_4SiC_4 material (5.6%), the effect of porosity/density on the hardness results can be neglected.

The elastic modulus of the sample S1650 was slightly lower than that of the S1600 and S1650-C samples (Table 1). This was probably caused by the presence of a large amount of the secondary phases with low elastic modulus in the S1650 sample. The amorphous silicate-like phases possess a low elastic modulus, which would decrease the elastic modulus of the whole composite body [40].

Table 1 shows the fracture toughness of the SiC/ Al_4SiC_4 composites sintered at different temperatures. The fracture toughness of the composite sintered with Y additive at 1650 ℃ (4.9 ± 0.2 MPa·$m^{1/2}$) was significantly higher than the fracture toughness of both the composite sintered without Y additive (2.7 ± 0.09 MPa·$m^{1/2}$) and the pure Al_4SiC_4 monolith (2.2 ± 0.2 MPa·$m^{1/2}$). Such a relatively high fracture toughness of the S1650 sample can be attributed mainly to its high density, and the presence of the fine SiC particles. Furthermore, the chemistry of the grain boundary phases would also play an important role in toughening, as the weak interface could improve fracture toughness. In order to understand the fracture mechanisms, the propagation of the indentation cracks and the fractured surfaces of the composites sintered at 1650 ℃ (with and without Y additive) were observed by SEM.

Figures 7(a) and 7(c) show the BSE images of the indentation crack paths in the S1650 and S1650-C samples. The straight crack path and mainly transgranular fracture were observed in the S1650-C sample (Fig. 7(c)). The corresponding fracture surface was relatively smooth (Fig. 7(d)). Transgranular failure was the main fracture mechanism, which suggests a low fracture toughness of the material.

On the other hand, some typical toughening mechanisms, such as crack deflection and crack bridging, were observed in the sample S1650 (Fig. 7(a)). The crack bridging and crack deflection inhibited the crack growth, resulting in a high fracture toughness of the material. The corresponding fracture surface was relatively rough (Fig. 7(b)), consisting of both the intergranular and transgranular failure modes. The intergranular fracture should constitute a major contribution to the high fracture toughness obtained for the material [25]. The intergranular fracture of S1650 was indicated by the holes as shown in Fig. 7(b). The holes were formed by the pullout of the SiC and some

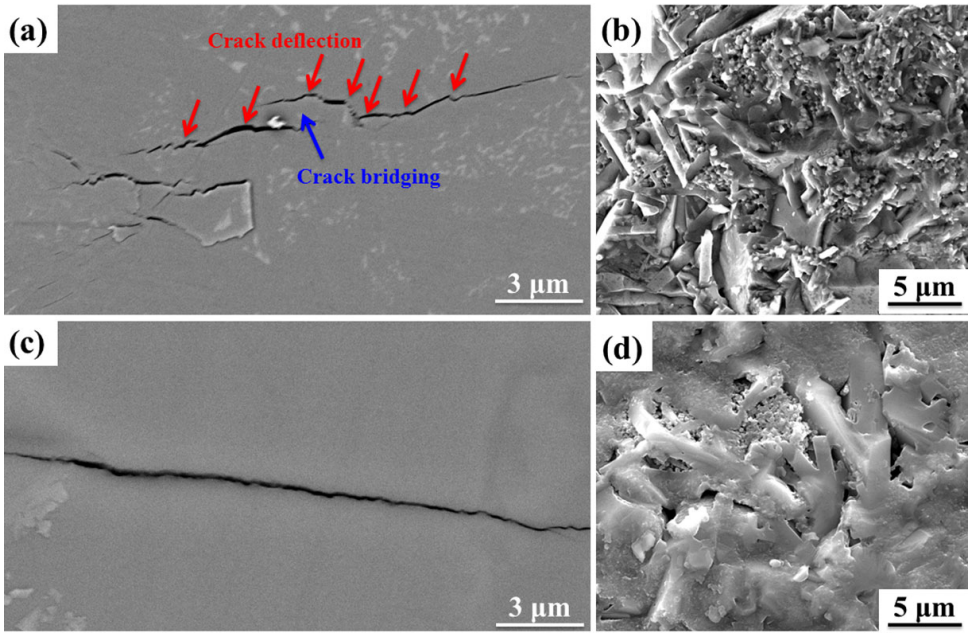

Fig. 7 Typical SEM microstructure images of (a, b) S1650 and (c, d) S1650-C samples: (a, c) the crack propagation path after the indentation test; (b, d) the fracture surfaces.

Al_4SiC_4 grains, indicating a relatively low interfacial strength at the grain boundaries [40]. Such a weak interface led to the more tortuous crack path and the intergranular fracture in the SiC/Al_4SiC_4 composite sintered with Y additive at 1650 ℃.

The SEM analysis also revealed that the size of the Al_4SiC_4 grains was significantly different than that of the SiC grains, leading to a broad grain size (bimodal) distribution of the composite. In general, the bimodal grain size distribution is beneficial for the increase in the number of crack deflection events and other toughening mechanisms [41]. The crack deflection consumed more fracture energy, resulting in a higher fracture toughness of the material.

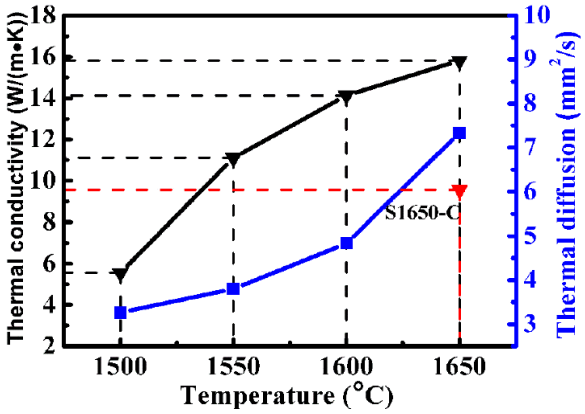

Fig. 8 Thermal conductivity of the SiC/Al_4SiC_4 composites sintered at different temperatures with and without Y sintering additive (S1650-C).

3. 4 Thermal properties

Figure 8 shows the thermal conductivity of the SiC/Al_4SiC_4 composites sintered at different temperatures. The thermal conductivity increased with the increasing sintering temperature. The thermal conductivity of the S1500 sample was only 5.6 W/(m·K), whereas it significantly increased to 15.8 W/(m·K) for the specimen S1650. On the other hand, the thermal conductivities of the monolithic Al_4SiC_4 material and the composite without Yadditive (S1650-C) were 7.8 and 9.6 W/(m·K), respectively. Thus, the thermal conductivity of Al_4SiC_4 was significantly improved by the incorporation of the fine grained SiC with high intrinsic thermal conductivity, as well as by the beneficial effect of the Y sintering additive.

The thermal conductivity of ceramics is determined by the density, grain size, as well as phase composition of the specimens. The S1650 specimen showed the highest density among all of the investigated materials. Moreover, the heat in the SiC/Al_4SiC_4 composites is mainly transferred by phonons, due to the lack of electronic conductivity of SiC and Al_4SiC_4 [25]. The material with a smaller grain size contains more grain boundaries per volume unit, which results in the phonon scattering at the grain boundaries. This significantly decreases the thermal conductivity of the material. The

S1650 sample contained much larger SiC grains (304 ± 33 nm) when compared to the samples of S1600 (153 ± 25 nm) and S1650-C (131 ± 16 nm), which can well explain the higher thermal conductivity of the S1650 sample. It should also be mentioned that there was obviously more liquid phase formed at the grain boundaries and grains junctions in the S1650 sample, when compared to the samples S1600 and S1650-C. A higher amount of the grain boundary phases may be harmful to the thermal conductivity of the materials. In the present study, however, the large grain size of SiC and the high density of the S1650 sample obviously eliminated the negative effect of the higher fraction of the grain boundary phases. It can be concluded that the highest thermal conductivity of the SiC/Al_4SiC_4 composite sintered with Y additive at 1650 ℃ was attributed to its high relative density and the relatively large grain size, resulting in less phonon scattering.

4 Conclusions

The highly dense SiC/Al_4SiC_4 composites (98.6%) with the improved hardness (16.3 ± 0.6 GPa), fracture toughness (4.9 ± 0.2 $MPa·m^{1/2}$), and thermal conductivity (15.8 $W·m^{-1}·K^{-1}$) were fabricated by SPS at a relatively low temperature of 1650 ℃. The materials were obtained by the *in-situ* reaction sintering of the starting mixture of PCS, Al, and 5 wt% Y sintering additive. Both, the phase transformation of $Y_3Si_2C_2$ at the temperatures around 1560 ℃, and the liquid phase formation in the $SiC(SiO_2)–Al_2O_3–Y_2O_3$ systems at around 1650 ℃ significantly promoted the densification of SiC/Al_4SiC_4 composites. The *in-situ* reactions led to the formation of fine grained SiC particles in the microstructure. The hardness, elastic modulus, fracture toughness, and thermal conductivity of Al_4SiC_4 ceramics were significantly improved by the incorporation of the SiC particles. The improved mechanical properties and thermal conductivity of the SiC/Al_4SiC_4 composite sintered at 1650 ℃ were attributed to its high density, appropriate grain size and bimodal grain size distribution, as well as to the appropriate grain boundary structure.

Acknowledgements

This study was supported by the National Natural Science Foundation of China (Grant Nos. 11975296 and 51811540402), and the Natural Science Foundation of Ningbo City (Grant No. 2018A610001). This work was also supported by the Slovak Research and Development Agency under the contract No. APVV-SK-CN-2017-0040. Peter TATARKO gratefully acknowledges the financial support of the project APVV-17-0328.

References

[1] Liao T, Wang JY, Zhou YC. Atomistic deformation modes and intrinsic brittleness of Al_4SiC_4: A first-principles investigation. *Phys Rev B* 2006, **74**: 174112.

[2] Xing XM, Li B, Chen JH, *et al*. Formation mechanism of large size plate-like Al_4SiC_4 grains by a carbothermal reduction method. *CrystEngComm* 2018, **20**: 1399–1404.

[3] Sun L, Gao YM, Yoshida K, *et al*. Prediction on structural, mechanical and thermal properties of Al_4SiC_4, Al_4C_3 and 4H-SiC under high pressure by first-principles calculation. *Mod Phys Lett B* 2017, **31**: 1750080.

[4] Xing XM, Chen JH, Bei GP, *et al*. Synthesis of Al_4SiC_4 powders via carbothermic reduction: Reaction and grain growth mechanisms. *J Adv Ceram* 2017, **6**: 351–359.

[5] Le-Tran HL, Sarigiannidou E, Gélard I, *et al*. Vaporization and condensation in the Al_4C_3-SiC system. *J Eur Ceram Soc* 2017, **37**: 4475–4482.

[6] Chen JH, Zhang ZH, Mi WJ, *et al*. Fabrication and oxidation behavior of Al_4SiC_4 powders. *J Am Ceram Soc* 2017, **100**: 3145–3154.

[7] Huang XX, Wen GW, Cheng XM, *et al*. Oxidation behavior of Al_4SiC_4 ceramic up to 1700 ℃. *Corros Sci* 2007, **49**: 2059–2070.

[8] Yamamoto O, Ohtani M, Sasamoto T. Preparation and oxidation of Al_4SiC_4. *J Mater Res* 2002, **17**: 774–778.

[9] Wen GW, Huang XX. Increased high temperature strength and oxidation resistance of Al_4SiC_4 ceramics. *J Eur Ceram Soc* 2006, **26**: 1281–1286.

[10] Yu C, Deng CJ, Zhu HX, *et al*. Slag corrosion resistance of Al_4SiC_4. *Int J Mater Res* 2017, **108**: 249–252.

[11] Yu C, Cheng KR, Ding J, *et al*. Synthesis and some properties of Al_4SiC_4-Al_4O_4C composites. *Ceram Int* 2018, **44**: 17154–17159.

[12] Magnani G, Galvagno S, Sico G, *et al*. Sintering and mechanical properties of β-SiC powder obtained from waste tires. *J Adv Ceram* 2016, **5**: 40–46.

[13] Fu CL, Yang Y, Huang ZR, *et al*. Investigation on the laser ablation of SiC ceramics using micro-Raman mapping technique. *J Adv Ceram* 2016, **5**: 253–261.

[14] Wang HL, Gao ST, Peng SM, *et al*. KD-S SiC_f/SiC composites with BN interface fabricated by polymer infiltration and pyrolysis process. *J Adv Ceram* 2018, **7**: 169–177.

[15] Liu GW, Zhang XZ, Yang J, *et al*. Recent advances in joining of SiC-based materials (monolithic SiC and SiC_f/SiC composites): Joining processes, joint strength, and interfacial behavior. *J Adv Ceram* 2019, **8**: 19–38.

[16] Zhou YC, Wan DT, Bao YW, *et al*. *In situ* processing and high-temperature properties of $Ti_3Si(Al)C_2$/SiC composites. *Int J Appl Ceram Technol* 2006, **3**: 47–54.

[17] Wan DT, Zhou YC, Bao YW, *et al*. *In situ* reaction synthesis and characterization of $Ti_3Si(Al)C_2$/SiC composites. *Ceram Int* 2006, **32**: 883–890.

[18] Zhang JF, Wu T, Wang LJ, *et al*. Microstructure and properties of Ti_3SiC_2/SiC nanocomposites fabricated by spark plasma sintering. *Compos Sci Technol* 2008, **68**: 499–505.

[19] Inoue K, Yamaguchi A. Synthesis of Al_4SiC_4. *J Am Ceram Soc* 2003, **86**: 1028–1030.

[20] Lee SH, Oh HC, An BH, *et al*. Ultra-low temperature synthesis of Al_4SiC_4 powder using spark plasma sintering. *Scr Mater* 2013, **69**: 135–138.

[21] Hasegawa M, Itatani K, Aizawa M, *et al*. Low-temperature synthesis of aluminum silicon carbide using ultrafine aluminum carbide and silicon carbide powders. *J Am Ceram Soc* 1996, **79**: 275–278.

[22] Oscroft RJ, Thompson DP. Influence of oxygen on the formation of aluminum silicon carbide. *J Am Ceram Soc* 1992, **75**: 224–226.

[23] Lee JS, Lee SH, Nishimura T, *et al*. Hexagonal plate-like ternary carbide particulates synthesized by a carbothermal reduction process: Processing parameters and synthesis mechanism. *J Am Ceram Soc* 2009, **92**: 1030–1035.

[24] Yu C, Yuan WJ, Deng CJ, *et al*. Synthesis of hexagonal plate-like Al_4SiC_4 from calcined bauxite, silica and carbon black. *Powder Technol* 2013, **247**: 76–80.

[25] Shao JQ, Li M, Chang KK, *et al*. Fabrication and characterization of SPS sintered SiC-based ceramic from $Y_3Si_2C_2$-coated SiC powders. *J Eur Ceram Soc* 2018, **38**: 4833–4841.

[26] Zhou YC, Xiang HM, Dai FZ. Y_5Si_3C and $Y_3Si_2C_2$: Theoretically predicted MAX phase like damage tolerant ceramics and promising interphase materials for SiC_f/SiC composites. *J Mater Sci Technol* 2019, **35**: 313–322.

[27] Pan Z, Fabrichnaya O, Seifert HJ, *et al*. Thermodynamic evaluation of the Si-C-Al-Y-O system for LPS-SiC application. *J Phase Equilib Diffus* 2010, **31**: 238–249.

[28] Hasegawa Y, Okamura K. Synthesis of continuous silicon carbide fibre. *J Mater Sci* 1983, **18**: 3633–3648.

[29] Birot M, Pillot JP, Dunogues J. Comprehensive chemistry of polycarbosilanes, polysilazanes, and polycarbosilazanes as precursors of ceramics. *Chem Rev* 1995, **95**: 1443–1477.

[30] Anstis GR, Chantikul P, Lawn BR, *et al*. A critical evaluation of indentation techniques for measuring fracture toughness: I, direct crack measurements. *J Am Ceram Soc* 1981, **64**: 533–538.

[31] Unlu MD, Goller G, Yucel O, *et al*. Processing and mechanical characterisation of monolithic silicon carbide ceramic consolidated by spark plasma sintering (SPS). *Int J Mater Res* 2013, **104**: 1240–1246.

[32] Volz E, Roosen A, Hartung W, *et al*. Electrical and thermal conductivity of liquid phase sintered SiC. *J Eur Ceram Soc* 2001, **21**: 2089–2093.

[33] Carotenuto G, Gallo A, Nicolais L. Degradation of SiC particles in aluminium-based composites. *J Mater Sci* 1994, **29**: 4967–4974.

[34] Yu C, Wu ZM, Ding J, *et al*. Effect of Al_4SiC_4 additive on the fabrication and characterization of recrystallized SiC honeycomb ceramics. *Ceram Int* 2019, **45**: 16612–16617.

[35] Lee JS, Ahn YS, Nishimura T, *et al*. Ultra-low-temperature sintering of nanostructured β-SiC. *J Am Ceram Soc* 2011, **94**: 324–327.

[36] Xu K, Zou HK, Chang KK, *et al*. Thermodynamic description of the sintering aid system in silicon carbide ceramics with the addition of yttrium. *J Eur Ceram Soc* 2019, **39**: 4510–4519.

[37] Liang HQ, Yao XM, Huang ZR, *et al*. *In situ* analysis of the liquid phase sintering process of alpha-SiC ceramics. *J Inorg Mater* 2016, **31**: 443.

[38] Falk LKL. Microstructural development during liquid phase sintering of silicon carbide ceramics. *J Eur Ceram Soc* 1997, **17**: 983–994.

[39] German RM, Suri P, Park SJ. Review: Liquid phase sintering. *J Mater Sci* 2009, **44**: 1–39.

[40] Sciti D, Guicciardi S, Bellosi A. Effect of annealing treatments on microstructure and mechanical properties of liquid-phase-sintered silicon carbide. *J Eur Ceram Soc* 2001, **21**: 621–632.

[41] El-Atwani O, Quach DV, Efe M, *et al*. Multimodal grain size distribution and high hardness in fine grained tungsten fabricated by spark plasma sintering. *Mater Sci Eng: A* 2011, **528**: 5670–5677.